Domain wall dynamics and Barkhausen jumps in thin-film permalloy microstructures

Shuqiang Yang and J. L. Erskine
Department of Physics, University of Texas at Austin, Austin, Texas 78712, USA
(Received 13 July 2004; revised manuscript received 1 July 2005; published 16 August 2005)

Domain wall jump-amplitude and velocity distributions associated with Barkhausen jumps in a 300-Å-thick thin-film permalloy and a 200×200 $(\mu m)^2\times220$-Å-thick permalloy sample microstructrue are measured using a high-speed magneto-optic Kerr effect polarimeter. The jump-amplitude and velocity distributions are obtained for applied-field sweep rates from 0.9 Oe/s to 6.3×10^4 Oe/s. The velocity distributions exhibit statistical properties consistent with the stochastic description of field-driven domain wall motion developed by ABBM [B. Alessandro, C. Beatrice, G. Bertotti, and A. Montorsi, J. Appl. Phys. **68**, 2901 (1990)]. Averaged velocity distributions exhibit the expected increase of dynamic coercivity as the sweep rate is increased, and the maximum domain wall velocity measured as a function of the applied field at the stochastic depinning threshold is shown to be governed by the mobility limit imposed by local spin damping. The averaged velocity $\langle v(H-H_0)\rangle$ obtained from the distributions is observed to depart from the commonly accepted linear-dependence model, especially at higher drive-field sweep rates. This departure is interpreted as an indication of a sweep-rate-dependent mobility. Sweep-rate-dependent jump-amplitude distributions $P(\Delta M)$ versus ΔM are obtained from the Barkhausen effect data. These distributions exhibit power-law behavior with a sharp cutoff at large values of ΔM. Attempts to reconcile the measured jump-amplitude distributions and sweep-rate-dependent exponents with various models of universal scaling are described. Power-law fits to $P(\Delta M)$ distributions measured to optimize temporal resolution (required for the velocity-distribution studies) yield a sweep-rate-dependent exponent that varies from $\beta=1.45\pm0.05$ to $\beta=1.0$ as dH/dt is varied from 25 Oe/s to 6.3×10^4 Oe/s. This range of sweep-rate-dependent β agrees with the ABBM model and is consistent with the sweep-rate dependence exponent rule that predicts linear sweep-rate scaling for the adiabatic value $\beta=3/2$ [R. A. White and K. A. Dahmen, Phys. Rev. Lett. **91**, 085702 (2003)]. Additional experiments on both 300-Å-thick continuous films and the same microstructures optimized for ΔM sensitivity yield a more accurate value of β ($\beta=1.33\pm0.01$), which corresponds to a CZDS model ($\beta=4/3$) [C. Cizeau, S. Zapperi, G. Durin, and H. E. Stanley, Phys. Rev. Lett. **79**, 4669 (1997); Phys. Rev. B **58**, 6353 (1998)]. Adiabatic limit values of β determined from all of the experiments are definitively outside the range $\beta\sim1.0$ for self-organized criticality in a two-dimensional system [P. Bak, C. Tang, and K. Wiesenfeld, Phys. Rev. Lett. **59**, 381 (1987)], and also appear to be inconsistent with experimental results for 900 Å Fe films on MgO in which $\beta=1.1$ was obtained from rescaled $P(\Delta M)$ distributions [E. Puppin, Phys. Rev. Lett. **84**, 5415 (2000)]. The sweep-rate dependence of β determined in a system that manifests an adiabatic limit of β that is not equal to 3/2 also violates the model of White and Dahman that prohibits sweep-rate-dependent scaling for $\beta=4/3$.

DOI: 10.1103/PhysRevB.72.064433 PACS number(s): 75.60.Ej

I. INTRODUCTION

The random changes in magnetization resulting from irreversible stochastic motion of domain walls (DWs) during field-driven magnetization reversal are known as the Barkhausen effect (BE). A detailed description of the BE, and closely related ferromagnetic hysteresis, at the level of nanometer-scale interactions of DWs with lattice defects, impurities, and surface/interface features that can act as DW pinning centers continues to present difficult challenges. However, phenomenological descriptions of the BE[1–4] and magnetic hysteresis[5–7] now provide remarkably simple expressions for DW velocities, BE jump-amplitude distribution functions, and various scaling laws that can be experimentally tested. Specifically, power-law functions describing probability distributions, including drive-frequency-dependent scaling behavior associated with the BE, have been measured in bulk samples and in many cases have been shown to be in good agreement with theoretical predictions;[1–3] related experiments have explored correlation effects in BE avalanches and concepts of self-organized criticality.[8] Nearly all of these results have been obtained using bulk samples in which eddy-current damping governs DW mobility and in which the probed sample volume is large $(1\ mm)^3$ and determined by the induction pick-up coil technique used in the experiments.

The BE experiments reported in this paper are carried out in a different regime using thin-film microstructures in which eddy-current damping is negligible, and where the probed sample volume is precisely defined and much smaller than a typical bulk-sample grain size $(100\ \mu m)^3$. The absence of eddy-current damping in thin films and thin-film-based structures permits very high DW velocities during Barkhausen jumps (BJs) that are limited (as demonstrated in this paper) by local spin-damping mechanisms. This feature plays a role in determining sweep-rate-dependent exponents that characterize BJ statistical distributions and may help account for the striking differences apparent from a simple visual comparison (p. 17, Ref. 1) of BN spectra of bulk and thin-film samples: BJ spectra for thin films exhibit very sharp peaks of short duration with no detectable structure, whereas bulk ma-

terials produce BJ spectra with jagged structure characteristic of avalanche behavior.

The results presented in this paper are discussed within the framework of two models: a domain dynamics model developed by Alessandro, Beatrice, Bertotti, and Montorsi (ABBM)[2] and a generalization of the ABBM model (that includes dimensionality) described by Cizeau, Zapperi, Durin, and Stanley (CZDS).[3] The ABBM model provides a good basis for describing the velocity distributions, based on a mobility equation, and the power-law sweep-rate dependences that describe jump-amplitude distributions. However, the low sweep-rate (adiabatic) value of the velocity distribution exponent obtained from our experimental results suggests that the thin films and thin-film microstructures studied in work reported in this paper behave as two-dimensional (2D) systems which are more appropriately described by the CZDS model. A starting point for summarizing the underlying assumptions and features of the ABBM model and understanding the experimental data presented in this paper is the classic result obtained by Williams, Shockley, and Kittel[9] in which it was shown that the average field-driven DW motion at slow sweep rates is governed by a mobility relationship,

$$\langle v_{\mathrm{DW}} \rangle = \xi (H - H_0), \tag{1}$$

where H is the external applied field and H_0 is a threshold field that includes internal counterfields of various origins including demagnetizing fields, DW interactions with pinning centers, and DW-DW interactions. The parameter ξ is the DW mobility. In thick metallic ferromagnetic films, DW damping is governed by eddy currents[9] with energy dissipation that scales as $M_s^2 v^2 \Delta x^2 / \rho$ and mobility that scales as $\rho/(M_s \Delta x)$, where M_s= saturation magnetization, Δx=thickness, and ρ=resistivity. In very thin films (Δx < a few hundred Å), the mobility increases until limited by a different (local) damping mechanism which we show to be the intrinsic spin-damping mechanism that is incorporated in the Landau-Lifshits-Gilbert (LLG) equations in the form of a dimensionless parameter, α_G.

The ABBM[2] model generalizes Eq. (1) by postulating that the instantaneous DW velocity is governed by a similar equation,

$$v_{\mathrm{DW}} = \xi' [H - (H_{\mathrm{dm}} + H_p)], \tag{2}$$

where the geometry-dependent demagnetizing field H_{dm}, is separated from a random component H_p that includes all short-range counterfield contributions. The mobility parameter ξ' in Eq. (2) should be viewed as a statistical parameter with a maximum value ξ'_{max} governed by a suitable spin-damping mechanism. The pinning field H_p is assumed to exhibit statistical properties governed by details of the local pinning potentials that inhibit DW motion. The DW motion resulting from a uniformly increasing applied field (dH/dt =const) can be obtained analytically from this model yielding, among other predictions, scaling functions[3,4] that govern the distribution of DW velocities (v), Barkhausen jump (BJ) amplitudes (ΔM), and durations ($\Delta \tau$),

$$P(v) = v^{-\alpha} f(v/v_0), \quad \alpha = 1 - c, \tag{3}$$

$$P(\Delta M) = (\Delta M)^{-\beta} f(\Delta M / \Delta M_0), \quad \beta = 3/2 - c/2, \tag{4}$$

$$P(\Delta \tau) = (\Delta \tau)^{-\gamma} f(\Delta \tau / \Delta \tau_0), \quad \gamma = 2 - c, \tag{5}$$

where $c \propto dH/dt$ is a dimensionless parameter that characterizes the sweep rate, and $f(\mu)$ is a cutoff function. The parameters v_0, ΔM_0, and $\Delta \tau_0$ can be related to various material-dependent properties such as correlation lengths, conductivity, spin-damping parameters, and differential permeability.

In the ABBM model of DW motion, the parameter c determines the general characteristics of the probability distributions. In the adiabatic limit ($c \to 0$), the probability distributions for DW velocity, BJ amplitude, and duration become universal power-law functions. In the ABBM model, these exponents [from Eqs. (3)–(5)] are $\alpha = 1$, $\beta = \frac{3}{2}$, and $\gamma = 2$. In this limit, DW motion is characterized by intermittent jumps described by the distribution functions, Eqs. (3)–(5). In the limit $c \gg 1$, statistical effects are suppressed and the DW is assumed to move at a constant average velocity $\langle v \rangle$ described by Eq. (1). The condition $c = 1$ defines crossover from the regime ($c \ll 1$) of intermittent jumps to ($c \gg 1$) continuous motion. It is reasonable to assume that under suitable constraints or assumptions, Eqs. (1) and (2) would both provide an accurate description of DW processes. Our experiments indicate that the mobility equation, Eq. (1), can accurately describe averaged statistical distributions based on Eq. (2) by introducing an exponent q that allows nonlinear scaling of the applied field dependence, or by assuming that the mobility ξ depends on sweep rate.

Experiments on bulk magnetic samples carried out using flux pick-up coils are capable of detecting BE signals with sufficient sensitivity and dynamic range (over three decades in the jump-amplitude ΔM, for example) to accurately test the scaling function predictions of the ABBM model, Eqs. (3)–(5).[1–3,6,8] The pick-up coil technique measures flux changes that accompany BJs, and several assumptions and approximations are required to quantitatively interpret the measured BN jump amplitudes (pick-up coil voltage $\propto d\phi/dt$) in terms of absolute BJ volumes and velocities associated with DW motion.[10] In this paper, we report measurements of DW phenomena in thin-film permalloy microstructures that achieve sufficient temporal resolution and sensitivity to directly measure DW velocities of individual BJs and BN jump-amplitude distributions. These measurements permit a sensitive and direct experimental test of Eq. (2), as well as additional tests of the scaling laws Eqs. (3)–(5) and theories of universal scaling exponents on a spatial scale corresponding to 0.1% of the volume of a typical bulk-sample grain size. The films studied are thin enough (thickness=220 Å) to suppress eddy-current damping, and our experiments, therefore, probe all of these effects in a spin-damping regime that is different from eddy-current damping in bulk samples. We are able to demonstrate that the maximum value of the mobility parameter [ξ' in Eq. (2)] is governed in the thin-film limit by the local (gyromagnetic) damping mechanism. Our experimental results also demonstrate the limits of Eq. (1) (linear, nonstochastic model) for accurately describing DW dynamics, and explore selected

features of the distribution function exponents associated with Barkhausen effects in thin-film geometry.

II. EXPERIMENT

Domain wall motion and hysteresis loops were measured using a high-speed high-spatial-resolution magneto-optic Kerr effect (MOKE) polarimeter incorporated into a long-focal-length polarized-light microscope.[11] The polarimeter components were recently up-graded to optimize the sensitivity for BE measurements: relevant components include a 20 mW HeNe laser, small area (nanosecond response) silicon photodetectors, and wide-band low-noise preamplifiers. Under typical operating conditions [Figs. 1(c) and 1(d)], measurement of BE jump amplitudes, defined by $\Delta M/M$, with a signal-to-noise (S/N) ratio of slightly above 10:1, was achieved using an effective sampling time of 0.2 μs. Under these conditions, the noise floor was amplifier Johnson-noise limited, but near the shot-noise limit. The polarimeter response was calibrated by measuring the 10–90 % risetime of a square wave produced by modulating the laser intensity using a pockels cell (20 ns risetime, checked with a 1 ns photodiode and fast oscilloscope). The linear-ramp (sawtooth) magnetic field was produced by Helmholtz coils driven by a bipolar power supply. The Kerr effect signal was digitized by a fast oscilloscope (8 bit/1 GHz bandwidth) and transferred to a PC for processing. Digital averaging of data (binning of adjacent A/D samples) was used, in some cases, to improve the sensitivity [signal/noise ratio (S/N)] at the expense of temporal resolution in order to detect small BJs [compare noise floor of Figs. 1(a) and 1(b) for example].

The magnetic sample used in our experiments was a 200×200 $(\mu\text{m})^2\times220$-Å-thick microstructure of permalloy ($Ni_{80}Fe_{20}$) grown by ultrahigh-vacuum (UHV) electron-beam vapor deposition on a high-quality commercially polished Si(100) ±0.5° wafer. Standard e-beam lithography plus lift-off techniques were used to create several microstructures of slightly different sizes and shapes. Some experiments were also carried out on similarly prepared continuous 300-Å-thick films. Similar sample preparation and measurement techniques were recently used to study hysteresis loss scaling of permalloy microstructures over a wide drive-field frequency range (10^{-2}–10^6 Hz).[7] The sample used in the BE experiments reported in this paper exhibited the same typical low static coercivity (~0.5 Oe) and simple domain patterns common to thin-film permalloy microstructures.[7,13]

III. RESULTS AND DISCUSSION

Figure 1 displays representative measured changes in magnetization produced by BJs during field-driven magnetization reversal of the microstructured sample. The laser beam was focused to illuminate the entire sample area within the diameter that corresponds to half of the total flux. Therefore, all BJs created by the sample during magnetization reversal having amplitude above the noise floor were detected. Later it is demonstrated that the temporal resolution achieved in our experiments was sufficiently high to determine the maximum theoretical velocity of a DW during a BJ.

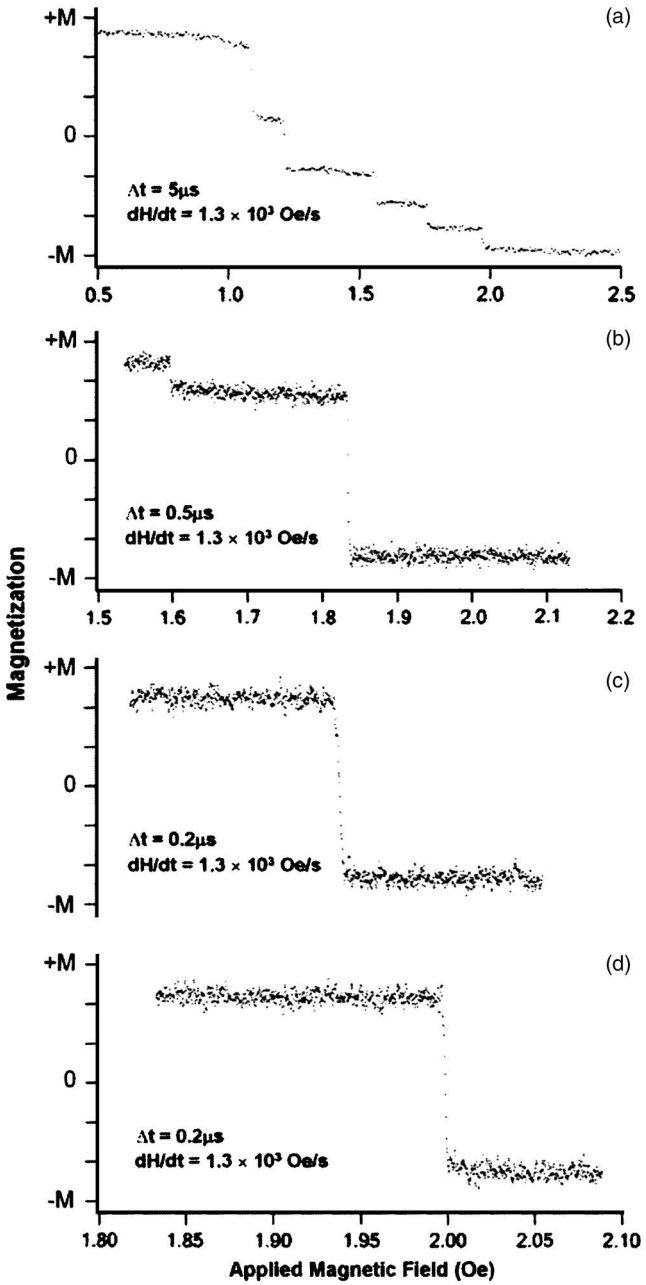

FIG. 1. Typical magnetic reversal transients $M(t)$ that exhibit Barkhausen jumps. The temporal resolution Δt parameter (each panel) corresponds to the integration time interval between $M(t)$ samples (each point). Note scale changes in horizontal axis (applied field). The magnetization axis corresponds to $\langle M_x\rangle$, the total average sample magnetization parallel to the applied field. The lower two panels C and D display single large fast (C) and faster (D) transients (v for panel D is ~150 m/s). The Johnson noise for (A) corresponds to $N\sim2\%$ $(2M)$; for (B) $N\sim10\%$ $(2M)$.

The well-defined spatial scale of the microstructured thin-film samples and the MOKE method employed to detect BJs offers the opportunity to carry out DW velocity measurements based on a model that relates DW velocity to measured values of ΔM: $v_{\mathrm{DW}}=(\Delta M/2M)^{\pi}L/\tau$, where L is a spatial scale parameter, and τ and $\Delta M/2M$ are the switching transient time and fractional change in magnetization result-

ing from a BJ. The parameter π permits analysis in terms of a one-dimensional model ($\pi=1$) in which a DW is assumed to sweep across the viewed area, or a two-dimensional model ($\pi=1/2$) in which a DW encloses an area where M abruptly changes. In the limit of large jumps ($\Delta M/2M \rightarrow 1$), both models yield the same calculated velocity.

In our experiments, the spatial scale L is determined by the sample size ($L=200$ μm) and $\Delta M/2M$ and τ are obtained directly from the BE jump amplitude (Fig. 1). We explored both model limits ($\pi=1$ and $\pi=1/2$) and observed no qualitative differences in the velocity distributions. Since the laser beam diameter was adjusted to cover the entire microstructure, $\pi=1/2$ was judged more appropriate for the smaller BJs and used to obtain the velocities described later and plotted in Fig. 4. We note that the distribution functions $P(\Delta M)$ (displayed in Fig. 2) and the scaling exponents obtained from them and discussed later are not affected by the choice of π. Obviously, an experimental velocity distribution function [i.e., Eq. (3)] would reflect model dependences, but the velocity exponents are not obtained or discussed in the present paper. The maximum DW velocity (discussed later) occurs for measured values of $\Delta M/2M \sim 1$, where model dependences do not matter. Also, in cases where the choice of π or the experimental noise floor, which limits detection of small BJs, could affect a conclusion (i.e., discussion related to Fig. 5), these dependences were explored.

Figure 2 displays log-log plots of BE jump-amplitude probability $P(\Delta M)$ versus jump-amplitude ΔM for linear-ramp sweep rates ranging from 13 Oe/s to 63 kOe/s (1 Hz–5 kHz sawtooth waveform). Each set of jump-amplitude probabilities $P(\Delta M)$ versus ΔM for a given value of sweep rate, dH/dt, was obtained from a computer-based search of about 10^4 half-cycle measurements of field-driven magnetization reversal. The smallest BE jump amplitudes recorded correspond to the threshold criteria $\Delta M \geqslant$factor of 2 above the noise floor. This criterion applied to the S/N level of typical ΔM transients measured at low sweep rates [for example, Fig. 1(a)] results in ΔM resolution of better than 5% and a dynamic range of 20. The binning procedure, described in Sec. II, was used to extend the S/N ratio for the 13 and 25 Oe/s drive-field frequency data [refer to $M(t)$ data displayed in Fig. 1(a)], which accounts for the extended range of $P(\Delta M)$ versus ΔM plots in Figs. 2(a) and 2(b). Each bin in the $P(\Delta M)$ histograms is based on well over 100 BJ events except for the last three or four bins (where ΔM is large and near $2M$). Therefore, the statistical errors in $P(\Delta M)$ values are below 10% except where indicated by error bars.

Curve fitting of the distributions using Eq. (4) (based on a strict power law without a cutoff function) yields the values of β and c displayed with each $P(\Delta M)$ distribution. The straight-line fits to at least 20 values of $P(\Delta M)$ for $\Delta M < 0.7(2M)$ corresponding to the determined values of β are indicated on the graphs, with error estimates that reflect the precision of the power-law fit based on chi-square analysis. The BE jump-amplitude probability distributions (Fig. 2) depart from power-law behavior over a very narrow range of jump amplitudes (cutoff regions are represented by only three or four data points) and the relative jump probability of these few points is low, resulting in significantly larger statistical errors indicated by error bars.

We conclude this section with a discussion of data presented in Figs. 2(b)–2(e) leading to the estimate $c \sim 1$ at $dH/dt \sim 6.3 \times 10^4$ Oe/s and $\beta=1.45\pm0.05$ at $c=0$ based on a power-law fit neglecting the cutoff behavior. Results for the extended-range $P(\Delta M)$ data [Figs. 2(a) and 2(b)] are discussed later. Due to the limited dynamic range of our experimental data at the sweep rates above 25 Oe/s, the $P(\Delta M)$ power-law scaling only covers about 1 decade for the higher sweep rates. While the precision of the power-law fit is good (refer to chi-square values, Table I), the accuracy of the value obtained from the fit can be strongly affected by the range of data available and by the cutoff function. We return to these issues after a brief discussion of relevant theoretical and experimental work on critical exponents presented in the subsection that follows.

The minor departures of $P(\Delta M)$ from power-law behavior (away from the cutoff region) are common features associated with microstructures. Lateral size constraints begin to limit the allowed domain configurations and this effect can add structure to log-log plots of $P(\Delta M)$ versus ΔM representing disruption of the power-law behavior of $P(\Delta M)$. In very small microstructures, the single-domain limit is reached in which $P(\Delta M)=1$ and $\Delta M=2M$. The size of the microstructure used in our experiments was selected to reduce these effects, allowing extraction of distribution function scaling exponents and comparison with those obtained from studies of bulk samples and continuous film systems.

The values of c and β displayed in Fig. 2 are estimated using the same one-decade range of ΔM values for each sweep rate by first noting that β is essentially constant (and described by $\beta=1.45\pm0.05$) for drive field frequencies $f=2$, 100, and 1000 Hz [Figs. 2(b)–2(d)], suggesting $c \ll \beta$, and then using $\beta=1.50-c/2$ with $\beta=1.0\pm0.05$ obtained from the 5000 Hz $P(\Delta M)$ fit [Fig. 2(e)] (yielding $c \sim 1$ at 5 kHz). Based on this analysis, our experiment detects frequency-dependent scaling of β over the sweep-rate range from 25 to 6.3×10^4 Oe/s, where $\beta=1.5$ corresponding to $c \ll 1$ for the lower sweep rates, and $\beta=1.0$ corresponding to $c=1$ at the highest sweep rate. This interpretation is consistent with the ABBM model exponent behavior, Eq. (4).

A. Critical exponents

The sweep-rate dependence of β and the $c \rightarrow 0$ limit estimate of ($\beta \sim 1.5$) obtained for our thin-film permalloy microstructure, demonstrated by the results presented in Fig. 2, merit further discussion. Despite the large number of publications describing BN phenomena, the number of reliable estimates of critical exponents is limited.[1] In addition, current understanding of sweep-rate dependences,[3,16] cutoff phenomena, dimensional crossover,[14,15] and generally the role of dimensionality in BN phenomena remains controversial. The recent review of Durin and Zapperi[1] presents a comprehensive picture of the current status of the subfield. Here we select and describe a few issues and recent publications that are most relevant to our new results, and then

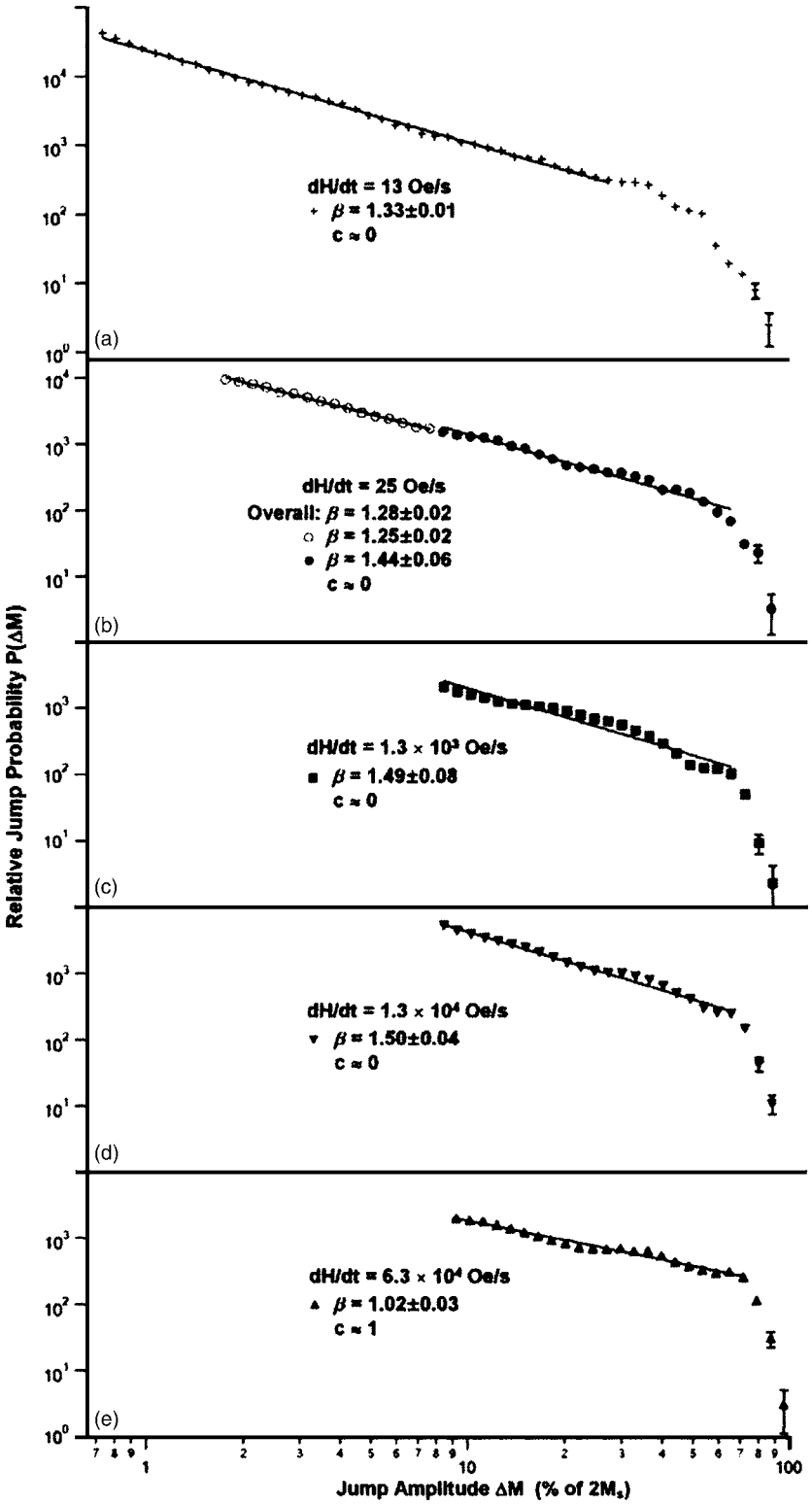

FIG. 2. Log-log plots of relative jump probability $P(\Delta M)$ vs jump amplitude ΔM. Values of scaling exponent β obtained from fitting data [using Eq. (4) without cutoff function] and values of sweep parameter c deduced from the values of β (refer to text) are displayed for each sweep rate. Open circles in panel B correspond to extension of the data set by the binning procedure described in the text. Symbol size represents error bars except where indicated. The data set displayed in panel A was obtained using a 50 mW solid-state laser and is described in Sec. III C. Note that the uncertainty assigned to the value of β is the precision of the fit based on chi-square values and not the accuracy of the determined value of β.

return to the result just described, i.e., our estimate of $\beta = 1.5$ at $c=0$ and its sweep-rate dependence.

The ABBM model[2] that yields the scaling functions Eqs. (3)–(5) is a single-degree-of-freedom model that neglects nucleation, interactions between DWs, and temperature effects, and is valid in the limit of low disorder. It has been used as a basis for understanding the measured value $\beta = 1.5$ at low sweep rates for a broad range of (mostly bulk) materials (refer to Table I in Ref. 1 and notes accompanying the table for details).

A generalization of the ABBM model introduced by Cizeau, Zapperi, Durin, and Stanley[3] (CZDS) and studied by others[15] yields the same $c=0$ limit scaling exponents

$$\beta = 2 - \frac{1}{\gamma}, \tag{6}$$

TABLE I. Power-law fits to data shown in Figs. 2 and 3. All fits cover ~1 decade, 20 values of $P(\Delta M)$ except where noted (by*). Chi-square values for top panel (power-law fit, no cutoff) show good precision for determination of β. Lower panel shows chi-square results for fits to two models: $\beta=1.5$ and $\beta=1.28$ without dH/dt scaling including the cutoff parameters indicated. Last entry (+) shows that chi-square fit improves significantly when $\beta=1$ is used for the highest sweep-rate distribution.

Power-law fit (excluding the last three points)		
dH/dt	β	Chi square
25 Oe/s	1.44±0.06	0.092
25 Oe/s*	1.28±0.02	0.14
1.3×10^3 Oe/s	1.49±0.08	0.20
1.3×10^4 Oe/s	1.50±0.04	0.047
6.3×10^4 Oe/s	1.02±0.03	0.032

Power-law fit (with cutoff, $M_o=83$, $\eta=10$)		
	Chi square	
dH/dt	$\beta=1.5$	$\beta=1.28$
25 Oe/s	1.3	0.98
1.3×10^3 Oe/s	1.3	1.8
1.3×10^4 Oe/s	0.74	0.55
6.3×10^4 Oe/s	0.88	0.38
	$\beta=1.0$	
6.3×10^4 Oe/s+	0.12	

$$\gamma=\frac{d+1}{2}, \tag{7}$$

where the more sophisticated model allows consideration of the effects of dimensionality d. A system governed by an upper critical dimension $d=3$ should yield $\gamma=2$, $\beta=\frac{3}{2}$ as in the ABBM model; for $d=2$, the exponents become $\gamma=\frac{3}{2}$, $\beta=\frac{4}{3}$.

A number of bulk and thin-film systems studied have also yielded values of the BE jump-amplitude exponent β that appear to fall into the $d=2$ universality class $\beta=\frac{4}{3}=1.33$ (refer to Table 1 of Ref. 1). A few recent examples will be discussed later in this paper.

Driving-rate effects[16] and dimensional crossover[17] have been studied theoretically in model systems that exhibit Barkhausen noise and avalanche behavior. The experimentally observed[3] linear dependence of scaling exponent on sweep rate [Eqs. (3)–(5)] for systems having $d=3$ yielding $\gamma=2$ and $\beta=\frac{3}{2}$ is explained[16] as resulting from "small avalanches disappearing from the distributions due to being absorbed into larger ones." According to this view of sweep-dependent exponents, an exponent inequality relationship exists that prohibits sweep-rate dependences for certain ranges of the value of universal scaling exponents. In other words, the adiabatic limit ($c\to0$) exponents are believed to govern finite-sweep-rate effects. Specifically for $\gamma<2$, no sweep-rate dependence is expected. From Eqs. (6) and (7) with $d=2$ yielding $\gamma=\frac{3}{2}$ and $\beta=\frac{4}{3}$, there should be no sweep-rate dependences, whereas for $d=3$, $\gamma=2$, and $\beta=\frac{3}{2}$, sweep-rate scaling is allowed.

The exponent inequality rule suggests that crossover between universality classes is an important factor in considering sweep-rate dependences in measured scaling exponents. The effects of dimensional crossover on scaling of avalanche distributions have been explored theoretically[17] based on the single-interface model. In this model, jump-amplitude histograms, $P(\Delta M)$, were obtained from simulations on an $L_x\times L_y\times\infty$ geometry "sample" in which the interface (DW) motion occurs along the infinite-length direction. Within these model simulations, the adiabatic limit exponent β for $P(\Delta M)$ distributions was found to vary from $\beta=1.06$ for $d=2(L_y\ll L_x)$ to $\beta=1.28$ for $d=3(L_y=L_x)$ representing different aspect ratios L_x/L_y for the DW cross section; significant variation of β was also found to occur as a function of the inverse size function $\sqrt{L_xL_y}$ that characterizes interface area. Based on these simulations, the cutoff function was also explored using an explicit (stretched exponential) form: $P(\Delta M)=(\Delta M)^{-\beta}e^{-(\Delta M/\Delta M_o)^{\eta}}$, where the simulations yielded fitted values for the exponent η falling in the range of 2.4–3.5 for about 60 sets of L_xL_y parameters. The jump-size distribution exponents β for $d=2$ and $d=3$ obtained from the above model are in good agreement with the corresponding results based on numerical simulations (in one, two, and three dimensions) using a nearest-neighbor cellular atomaton model[18] describing self-organized criticality, which yield $\beta=0.98$ for $d=2$ and $\beta=1.35$ for $d=3$. This limited overview of a few existing analytical models and numerical simulations that address BN scaling exponent properties serves as a basis for a closer examination of our results and a few related experiments, the objective being to place all of the results in some perspective.

Within the framework of the above outline of selected theoretical considerations, we briefly comment on a few experimental determinations of the exponent β that are related to our results. Wiegman[1,19] determined values of β for permalloy thin films covering a thickness range from 3000 to 500 Å using the induction pick-up coil method. The values are in the range $\beta\sim1.4$-1.6 for film thickness from 3000 to below 1000 Å, with much wider variation $\beta\sim1.3$–2.0 for films below 800 Å thickness where the sensitivity limit of the method is approached. Wiegman's experiments appear to be the only existing systematic experimental attempt to explore dimensional crossover effects in permalloy thin films. While the measured values of β in the thickness range 3000–1000 Å are compatible with $d=3$, the large variations in β obtained for thickness below 800 Å do not permit a meaningful comparison with our results or with various $d=2$ or $d=3$ values.

Puppin[12] reported $P(\Delta M)$ measurements of 900-Å-thick Fe films based on magneto-optical techniques in which the spot size was varied from 20 to 700 μm. By rescaling the measured distribution functions for various spot sizes to achieve a wide dynamic range of $P(\Delta M)$ versus ΔM, a value of $\beta\sim1.1\pm0.05$ was obtained. Corresponding measurements for permalloy microstructures[20] (20 μm squares, 800 Å thick) yielded $P(\Delta M)$ distributions that manifested strong finite-size effects at the cutoff region rendering accurate de-

termination of β difficult. Weak manifestations of these effects were noted in relation to our discussion of Fig. 2. Corresponding measurements[12] on larger permalloy structures (to 320 μm, 1600 Å thick) permitted an estimate ($\beta \sim 1.2$) based on approximately half a decade of $P(\Delta M)$ data excluding the cutoff region. More recently, Kim *et al.*[21] determined $\beta \sim 1.33 \pm 0.05$ for Co films ranging in thickness from 50 to 500 Å. In these experiments, the microscope field of view was varied, and the measured distributions were rescaled, as in Puppin's[12] work, to obtain $P(\Delta M)$ over a wide range of ΔM.

It is interesting to note that the value $\beta \sim 1.1$ obtained by Puppin[12] is compatible with the nearest-neighbor two-dimensional atomaton model numerical simulations[18] of self-organized criticality (SOC) in two dimensions, and that the value $\beta \sim 1.33$ obtained by Kim *et al.*[21] agrees with the 2D CZDS model[3] (or with the SOC 3D numerical simulations). However, neither of these experiments addressed the field sweep-rate dependence, and the procedure of rescaling $P(\Delta M)$ distributions determined using different fields of view have been shown to measure a different critical exponent than what is used for comparison.[1] At this point, it is not reasonable to draw any detailed conclusions regarding the nature of critical exponents in thin-film systems in relation to any of these models.

B. Additional curve fitting

The issues and results outlined in the previous subsection suggest a more detailed discussion of Fig. 2, and additional efforts to explore alternative interpretations of the scaling exponent result are in order. Two limitations of the experimental data account for the difficulty in obtaining accurate values of the exponent β: (i) the large statistical errors associated with the three to four points for large ΔM (cutoff region) resulting from relatively few events, and (ii) the limited dynamic range of the "power-law" region that is accessible without rescaling data. In addition, very little is known about the behavior of $P(\Delta M)$ in the cutoff region, and assumptions must be adopted for curve-fitting exercises that include the cutoff region. It may be possible (but difficult) to significantly improve both experimental limits. Here we attempt to examine, as carefully as possible, the existing data.

It was possible to extend the plot of $P(\Delta M)$ versus ΔM measured at the 25 Oe/s sweep rate by binning digital records, extending the total number of points from 26 to 41 (the effective dynamic range was improved about a factor of 2 from 20:1 to 50:1). Application of a power-law fit to 36 of the 41 points (neglecting the last three points in the cutoff region) yielded $\beta = 1.28 \pm 0.02$. The difference in the two values of β obtained from the 38-point fit and the 23-point fit is greater than the precision of either determination based on a least-squares analysis (Table I). The 38-point fit is judged to be more accurate. We are now faced with a dilemma: the value of β judged to be most accurate for low sweep rates is not consistent with $\beta = \frac{3}{2}$ (ABBM model[2]) and the exponent inequality relationship[16] which permits frequency-dependent scaling.

TABLE II. Power-law fits to independent data sets obtained using a more intense laser source and data reduction methodology that optimizes dynamic range (sensitivity) to ΔM rather than temporal resolution (which was emphasized in all other data sets presented in this paper). Left columns, sweep rate and value of β obtained from $P(\Delta M)$ distributions for the same 200×200 $(\mu m)^2$ microstructure used for other measurements (Figs. 1–3, Table I); right column, corresponding results for a continuous $(mm)^2$ scale 300-Å-thick permalloy film. Note that for the continuous film, the sweep-rate dependence of β is linear and that the departure of β from the adiabatic value occurs at a lower sweep rate for the thin film than for the microstructure film (because the jump durations are longer).

50 mW solid state laser			
200×200 $(um)^2$ sample		Continuous film	
Driving rate	Beta	Driving rate	Beta
13 Oe/s[a]	1.33	0.9 Oe/s	1.36
1.3×10^2	1.32	9	1.35
1.3×10^3	1.1	18	1.32
1.3×10^4	0.7	45	1.27
		67.5	1.22
		90	1.17
		112.5	1.11

[a]Data set shown in upper panel of Fig. 2.

Unfortunately, it is not possible, based on the currently achievable sensitivity of our experiment, to improve the accuracy of higher sweep-rate values of β significantly. At higher sweep rates, the effective sampling rate must also be increased and the effective dwell time (that determines the number of photons detected to measure ΔM) decreases and the resulting statistical noise increases. This increase in noise limits the sensitivity to small BE jump amplitudes. Several experiments (discussed in a following subsection) were carried out using a more intense (50 mW solid state) laser on the same permalloy microstructure and on a continuous 300-Å-thick permalloy thin film. The Fig. 2(a) $P(\Delta M)$ plot represents our data set obtained using the solid-state laser and slow sweep rate. These experiments yielded slight improvements in the sensitivity and an adiabatic value of $\beta (\beta = 1.33 \pm 0.01)$ in good agreement with the result $\beta = 1.28 \pm 0.02$ [Fig. 2(b) with binning], and measured values of β that clearly manifest sweep-rate-dependent scaling (discussed later in relation to Table II).

To further explore the possible interpretations of experimentally determined values of β based on the data presented in Figs. 2(b)–2(e), additional curve-fitting exercises were carried out (including the cutoff region) guided by the numerical simulations of scaling exponents and dimensional crossover that included some simulations of the cutoff function.[17] These simulations yielded $\beta \sim 1$ for $d=2$ and $\beta = 1.35$ for $d=3$ with cutoff exponents η for the stretched exponential in the range 2.4–3.5. A preliminary survey of parameter space relevant to our data revealed that $\beta = 1$ resulted in poor fits for all $P(\Delta M)$ results except for the highest sweep rate $dH/dt = 6.3 \times 10^4$ Oe/s and that cutoff parameters $M_o \sim 80$ and $\eta \sim 10$ yielded reasonable fits to the cutoff at all

values of dH/dt. While the value of the cutoff parameter η required to fit our data is significantly larger (over a factor of 2) than the range of values suggested by numerical simulations, the value we chose ($\eta=10$) permits a slightly better estimate of the power-law exponents by providing a more accurate representation of data points near the cutoff region.

Having eliminated $\beta\sim 1$ at low sweep rates (2D SOC case), we considered the following four possibilities with $M_o=83$ and $\eta=10$ fixed: (i) $\beta=1.28$ for all sweep rates; (ii) $\beta\sim 1.28$ for the lower sweep rates but $\beta=1$ for the high sweep rate; and (iii) $\beta=1.5$ for all sweep rates and $\beta=1.5$ for the lowest sweep rates but $\beta=1$ for the high sweep rate. We note that there is no reason to assume that the same cutoff function parameters should apply to different sweep rates, but without some rationale for selecting different cutoff function parameters, the above assumption seems justified. Table I summarizes how well the simulations match the data based on least-square fitting using the chi-square criteria. Figure 3 illustrates typical fits including the cutoff region. The primary conclusion is that reasonable fits to all four $P(\Delta M)$ versus ΔM data sets [Figs. 2(b)–2(e)] occur for either $\beta=1.5$ or $\beta=1.28$ as long as $\beta=1$ is used at the highest sweep rate. We cannot reasonably account for all of the $P(\Delta M)$ distributions, especially for the larger jumps, unless sweep-rate-dependent scaling of the exponent β is permitted and $\beta\sim 1$ is used at the highest sweep rate. Additional curve-fitting exercises applied to Figs. 2(b)–2(e) data were judged unlikely to provide a low sweep-rate value of β accurate enough to distinguish between $d=2$ and $d=3$ models or to resolve the dilemma emerging from the c-dependent $P(\Delta M)$ data. A definitive resolution of the issue regarding the relationship between sweep-rate-dependent scaling of β and its $c=0$ value will require development of more sensitive experimental techniques and extensive experiments. Ideally one would like to (i) explain in greater detail any effects on $P(\Delta M)$ resulting from microstructure size, (ii) achieve lower statistical error in the cutoff region enabling a more accurate account of these effects on the power law extracted from the fits, and (iii) achieve higher sensitivity at all sweep rates that would extend the $P(\Delta M)$ distributions far beyond the cutoff region, allowing a more accurate evaluation of the power-law exponent.

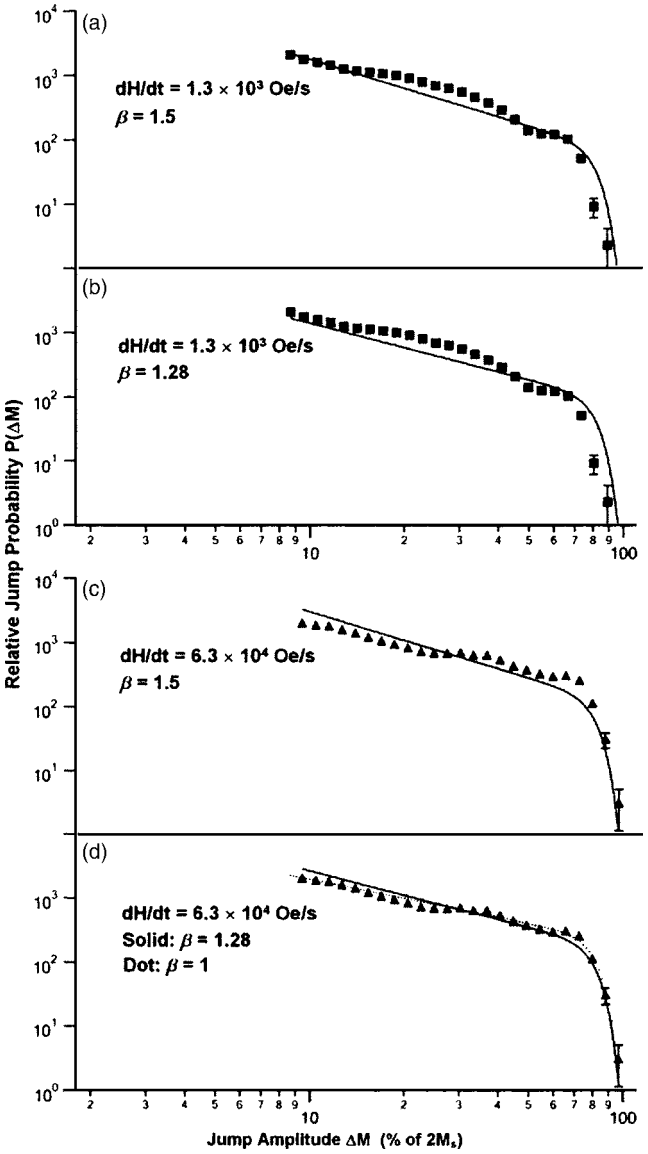

FIG. 3. Log-log plots of relative jump probability $P(\Delta M)$ vs jump amplitude ΔM (same as Fig. 2) with different fitting procedures applied (refer to Table I). Upper two panels display typical results obtained by fitting the lower three sweep-rate $P(\Delta M)$ distributions based on the same cutoff parameters (Table I) and (panel A) $\beta=1.5$ or (panel B) $\beta=1.28$. Lower two panels illustrate the problems of attempting to fit the high sweep-rate distribution using any exponent different from $\beta\sim 1.0$. A better fit to experimental points is possible with $\beta\sim 1$ using a sharper cutoff function [this requires a value of η larger than the range suggested by numerical simulations (Ref. 17)].

C. Additional experiments/sample-to-sample variation

In view of the issues raised in the previous subsections, additional experiments were performed on a separate continuous 300-Å-thick permalloy film and on the same 200×200 $(\mu\text{m})^2\times 220$-Å-thick microstructure using a more intense 50 mW solid-state laser. In these experiments, the data-acquisition strategy was optimized to detect small BJs at the expense of not being able to accurately measure the DW velocity during a BJ. The $P(\Delta M)$ distribution obtained using the more intense laser [Fig. 2(a)] yielded $\beta=1.33\pm 0.01$ at $dH/dt=13$ Oe/s. This value of β is consistent with the result $\beta=1.28\pm 0.02$ obtained using the binning procedure described earlier applied to the data obtained at $dH/dt=25$ Oe/s [Fig. 2(b)]. Sweep-rate-dependent studies of both the microstructure and continuous permalloy film yielded clear evidence of a sweep-rate-dependent exponent having an adiabatic value $\beta\sim 1.3$ that exhibited a strong sweep-rate variation to $\beta\sim 1$ at higher sweep rates.

Table II displays the sweep-rate-dependent values of β obtained using the more intense laser for both the continuous 300-Å-thick film and the 220-Å-thick 200×200 $(\mu\text{m})^2$ microstructure. [These values of β do not correspond to the measured velocity distributions described later in Fig. 4 or to $P(\Delta M)$ distributions in Fig. 2 except for the top panel.] A comprehensive account of these experiments that focus on

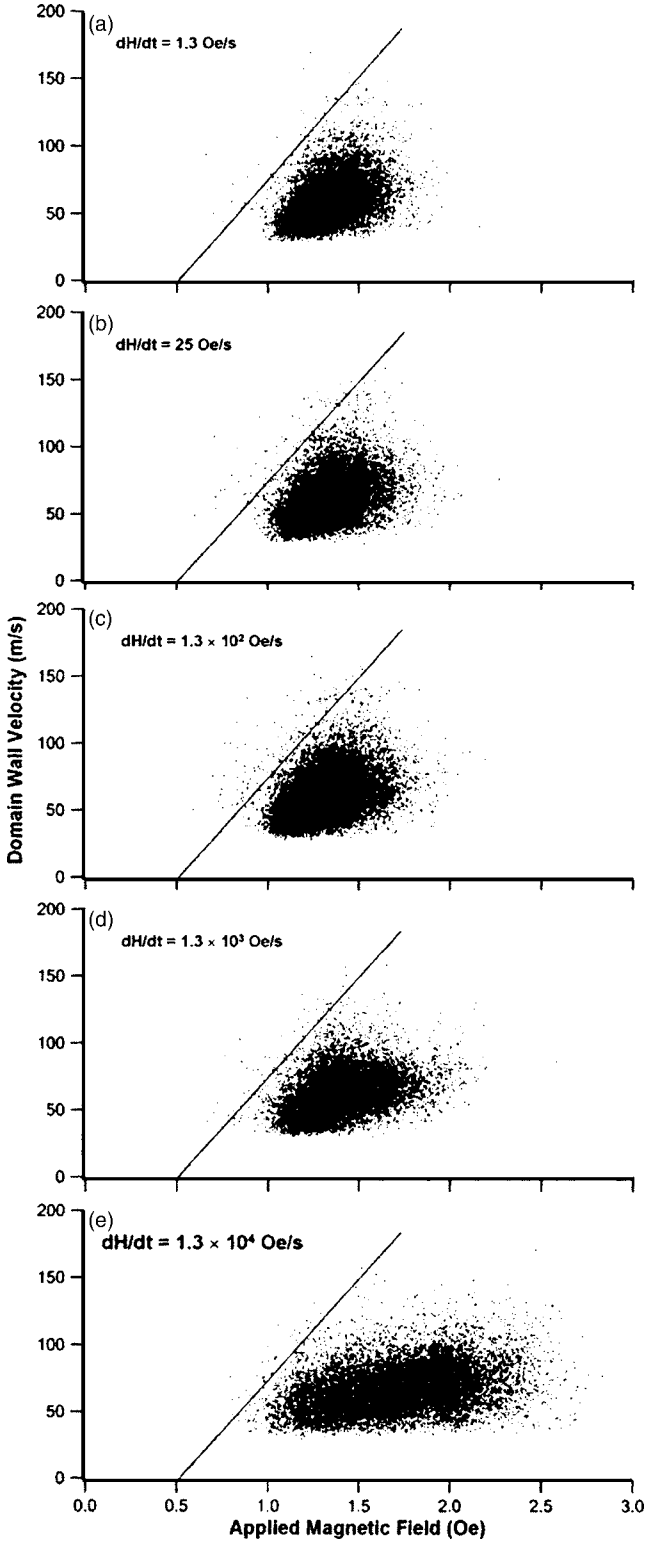

FIG. 4. Domain wall velocity and switching-field distributions associated with Barkhausen jumps as a function of drive-field sweep rate. Each point represents a DW velocity measurement (vertical scale) of a BE event that occurred at the applied field value (horizontal scale). Solid line, maximum estimated mobility $\zeta'_{\max}(H) \sim 150$ m/s Oe.

sweep-rate-dependent scaling and dimensional crossover is beyond the scope of the present paper and will be presented in a future publication. Based on the results presented in Tables I and II and in Figs. 2 and 3, we conclude the following regarding the exponent β for our permalloy films: (i) all data sets strongly support sweep-rate-dependent scaling of β; (ii) the most strongly supported value of β at low sweep rates (presumably the adiabatic limit) for permalloy films (and large microstructures) is $\beta = 1.33 \pm 0.01$, which is compatible with the $d=2$ CZDS result $\beta = \frac{4}{3}$; (iii) if the result $\beta = 1.5$ ($d=3$) obtained by Wiegman for permalloy films having thickness in the 1000–3000 Å range is valid, our results suggest dimensional crossover occurs in the thickness range between 1000 and 300 Å; and (iv) Table II presents strong experimental evidence supporting (linear) sweep-rate dependence of β for adiabatic values of β significantly different from $\beta = \frac{3}{2}$.

D. Domain wall velocity distributions and coercive force scaling

Figure 4 displays plots of DW velocity distributions obtained from $M(t)$ transients (as described in Sec. II) resulting from BJs at several sweep rates. These velocity distributions correspond to the $P(\Delta M)$ versus ΔM results (except top panel data obtained using the 50 mW laser) presented in Fig. 2. Each point corresponds to the measured DW velocity associated with a BJ that occurred at the instant the applied field reached the value H. The scatter plots are a graphical representation of Eq. (2). The distributions terminate at $H_{\rm dm}$ (the constant geometry-dependent term), and the range of $H > H_{\rm dm}$ where BJs are observed represents the statistical range of H_p values. The lower limit of DW velocity that can be determined is governed by the noise floor of the experiment. Digital signal averaging can be used to improve the signal-to-noise ratio, thus lowering the noise floor [compare Figs. 1(a)–1(c)], but the temporal resolution is reduced. This procedure can be used to add points to the scatter plot (mostly at low velocities), but when this is done, it is necessary to keep track of previously recorded transients to avoid double counting, which skews the distribution.

The maximum DW velocity that can be achieved during a BJ is governed by the mobility parameter $\xi'_{\max}$. Wall mobilities have recently been theoretically studied in permalloy films and stripline structures based on direct integration of the LLG equations.[22,23] The simulated mobilities depend on both the film thickness and stripline width, an apparent manifestation of the effects of geometrical constraints on dynamic DW structure. In addition, detailed studies of DW mobility in nanometer scale wires (both experiments and numerical simulations) manifest field-dependent mobilities that suggest multiple DW propagation regimes.[26,27] In the low-field regime, the DW velocity is described by Eq. (1) with a nearly constant high value of $\xi(\sim 50$ m/s Oe) that is consistent with the "Walker" solution of wall motion in a constant applied field. At a critical value of applied field $H_w \sim 4$ Oe, the spin dynamics changes into a new regime characterized by negative differential mobility over a range of applied fields extending to ~ 25 Oe, after which a second constant mobility

regime is established with a much lower value of $\xi(\sim 2.5$ m/s Oe). The "Walker" regime mobilities are governed by the values of the gyromagnetic constant and damping parameter, α_G, used in the LLG simulation of spin dynamics. In the stripline simulations,[23] an unrealistically high value of the damping parameter ($\alpha_G=0.3$) was used to reduce computational time, resulting in low values of computed DW mobility. A realistic estimate of the intrinsic maximum mobility $\xi'_{\max}$ can be obtained from the theoretical mobility of a domain wall, $\xi_t=\gamma\Delta/\alpha_G$, with characteristic wall width $\Delta_0=\Delta/\pi$ with Δ defined in terms of the points where the magnetization direction crosses ±90°. Using measured values of the gyromagnetic constant $\gamma=0.0179$ Oe^{-1} ns^{-1} (Ref. 24) and $\alpha_G=0.008$ (Ref. 25) for thin-film permalloy structures and an estimate of $\Delta=48$ nm for a Neél wall in a 31-nm-thick film,[22] $\xi'_{\max}\sim 110$ m/s Oe. The LLG simulations for 31-nm-thick permalloy films (based on an assumed $\alpha_G=0.05$) yield Neél wall mobility of 35 m/s Oe; scaling this result assuming the measured value of α_G ($\alpha_G=0.008$) yields $\xi'_{\max}>200$ m/s Oe. Based on these considerations, and on the apparent boundary of our experimental results, we assign $\xi'_{\max}\sim 150$ m/s Oe and indicate this limit on the scatter plots of Fig. 4 (solid lines with slope of $\xi'_{\max}$).

The qualitative features of the DW velocity scatter plots (Fig. 4) are consistent with the ABBM model [as represented by Eq. (2)] and with general features associated with the stochastic nature of the model predictions including the $c\propto dH/dt$-dependent distribution functions (Fig. 2). The well-defined scatter plot boundaries are consistent with the intrinsic mobility limit governed by local damping (slope$=\xi'_{\max}$), with the static coercivity of our permalloy sample (intercept at 0.5 Oe), and with the noise floor of the experiment (minimum measurable velocity). The *averaged* velocities also appear to be consistent with prior measured mobilities ($\xi\sim 38$ m/s Oe) of 30-nm-thick permalloy films[26–28] in the high mobility region. The jump amplitude distributions (Fig. 2) establish $c\sim 1$ at $dH/dt\sim 63$ kOe/s, therefore the upper four panels of Fig. 4 correspond to $c\ll 1$, and the distributions are remarkably similar (especially the upper three). It is apparent that the transition $c\to 1$ is accompanied by a change in the velocity distribution (lower two panels, Fig. 4).

Figure 5 establishes the compatibility of the measured BE distributions (Fig. 4) with multiple-loop averages that determine the sweep-rate dependence of the dynamic coercivity $H_c^*(\omega)$. This is important because later it is shown that the BE velocity distributions (Fig. 4) depart from the linear model of average DW velocity predicted by Eq. (1). In a recently reported study[7] of $H_c^*(\omega)$ for permalloy films and microstructures, we have shown that a frequency-dependent scaling function $H_c^*(\omega)$ under linear-ramp drive conditions can be obtained from a DW model adapted from Eq. (1),

$$H_c^*(\omega)=H_0+k(dH/dt)^{\varepsilon}. \tag{8}$$

Experimental data for $H_c^*(\omega)$ obtained using a similar evaporated-film permalloy microstructure [100×150 (μm)^2 $\times 300$ Å thick] follow this scaling function with $k=0.005$ and $\varepsilon=\frac{1}{2}$ for $1\leqslant dH/dt\leqslant 10^9$ Oe/s (9 decades) with noticeable departure from the adiabatic limit $H_c^*(\omega)\sim H_0$ occurring at about $dH/dt\sim 10^4$ Oe/s. The solid line in Fig. 5 represents $H_c^*(\omega)$ determined by multiple-loop averages over a very wide frequency range.[7] The five points plotted over the solid line represent averages of the five BJ distributions (Fig. 4) for each corresponding value of dH/dt. The agreement is excellent, showing that the averaged statistical data (BJ events at various H) obtained at a prescribed sweep rate reduce to the expected value of $H_c^*(\omega)$. Note that the measured frequency dependence of the magnetic energy loss (which is proportional to H_c^* for square loops driven to saturation) proves that eddy-current damping, which scales as ω^2, is not important for the thin-film samples used in these experiments. The scaling law, Eq. (8), and the measured $H_c^*(\omega)$ data represented in Fig. 5, and described in greater detail in Ref. 7, appear to be a general feature of thin-film magnetic response when eddy-current damping is suppressed provided that the $H_c^*(\omega)$ measurements are carried out over a sufficiently broad frequency range.[7,28–33]

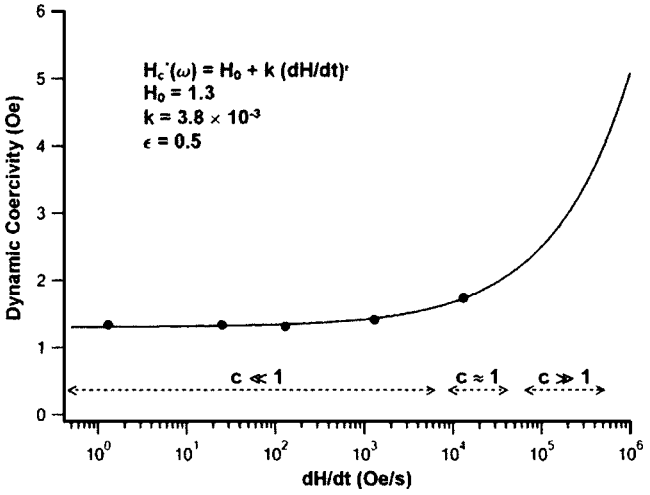

FIG. 5. Frequency-dependent scaling of dynamic coercivity $H_c^*(\omega)$. Solid line scaling function for $H_c^*(\omega)$ determined from CW measurements (Ref. 7); points, average of H_p values from Fig. 3 for each value of parameter c.

Several features of the experimental results (Fig. 4) provide striking evidence of the limitations of Eq. (1) in describing DW motion beyond the adiabatic ($c\to 0$) limit. The statistical nature of switching for $c<1$ is particularly evident in microstructures where $\Delta M/M$ can be large, yielding very large fluctuations in the nonaveraged DW velocities and switching fields. Also apparent from Fig. 4 is the departure of $\langle v(H-H_0)\rangle$ from the linear dependence on H that is inherent in Eq. (1). Figure 6 displays plots of $\langle v(H)\rangle$ obtained by averaging the measured velocity distributions around equally spaced values of H in the region of $H>H_{\rm dc}$. A significant departure from the linear relationship between v and $(H-H_0)$ is observed for all drive-field ramps studied (Fig. 4) especially at the larger values of H_p, and higher values of dH/dt. A more accurate description of the experimental data for $\langle v(H)\rangle$ obtained from averaging the measured distributions (Fig. 4) is obtained from the nonlinear version[1,7] of Eq. (1) that was used in obtaining the scaling function $H_c^*(\omega)$,

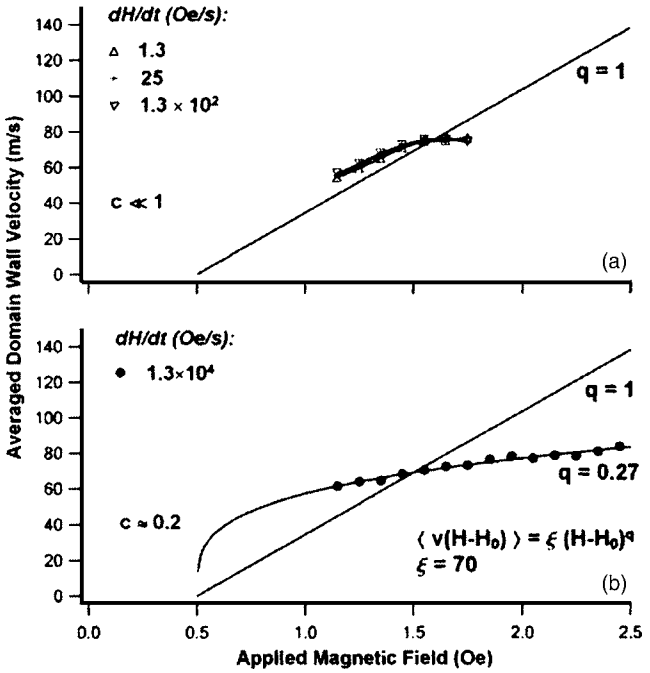

FIG. 6. Averages of DW velocities vs external field for two cases $c \ll 1$ (panel a) and $c \sim 0.2$ (panel b). Panel B displays two curves, a linear function [Eq. (1)] and a nonlinear function [Eq. (7)] fit to the $\langle v(H-H_0)\rangle$ data.

$$\langle v\rangle = \xi(H-H_0)^q \tag{9}$$

with $\xi \sim \xi_{\max}/2$ and $q=0.27$ [Fig. 5b]. Here we note that the form of the mobility equation given by Eq. (9) is used in descriptions of DW dynamics near a depinning transition.[1]

The nonlinear dependence of $\langle v(H-H_0)\rangle$ obtained by averaging the statistical velocity distributions is not a result of the sampling criteria used in generating the scatter plots (Fig. 4) from BJ data (Fig. 1). Similar nonlinear dependence was obtained by using velocity distributions resulting from BJs selected according to different ΔM criteria based on % change in ΔM relative to 100%: $\Delta M=30-35$, 40–45, 50–55, and 70–80 or using $\pi=1$. In addition, we have found no evidence that adding the missing small BJs associated with the finite noise threshold in the measurement would substantially alter the averages that yield $H_c^*(\omega)$ or $\langle v(H)\rangle$.

Departure of $\langle v(H)\rangle$ from the linear model [Eq. (1)] is not unexpected. Computer simulation[23] of average DW motion in thin (300 Å) magnetic stripline structures predicts mobility parameters [slope of $\langle v(H)\rangle$] that depart from linear behavior as H increases above H_0. These simulations were carried out using $\alpha_G \sim 0.3$ (strong damping) compared to the more realistic $\alpha_G \sim 0.008$ assumed for our permalloy samples. This accounts for the low values of calculated mobilities (~ 1 m/s Oe). However, essentially all of the calculated $v(H)$ plots in Ref. 23 (and specifically the plot for the 300-Å-thick 5000-Å-wide strip) can be fit by Eq. (7) with $q<1$. The variation of mobility versus H is attributed to dynamic changes in DW structure at larger field values.

Experiments[26] that directly measure the mobility parameter ξ clearly show that the mobility is H-dependent and exhibits dramatic negative differential behavior near H_w, the Walker breakdown field.[26,27] This effect is relevant to frequency-dependent studies of DW velocities at constant applied field amplitude because at higher frequencies the switching (on average) occurs at higher values of H, as shown by the distribution functions in Fig. 4, and the mobility parameter [slope of $v(H)$ curve] is no longer constant as H approaches H_w.

It is interesting to note that Monte Carlo simulation[34] of magnetization reversal in ultrathin Fe/W(110) predicts $v(H)$ behavior consistent with Eq. (7) but with $q>1$. Specifically, for 1.5 ML films, the film consists of nanometer-scale 2-ML-thick islands in a continuous 1 ML epitaxial film. In this system, thermal effects play a dominant role because the BJ volume is very small, and governed by the island size. Calculated $M(t)$ results for this ultrathin film system manifest BJ behavior very similar to our Fig. 1 data; also, power scaling law of $H_c^*(\omega)$ is predicted, and the average calculated velocity (for 1.56 ML films) $\langle v(H)\rangle$ can be fit by Eq. (7) with $q \sim 2$. Based on these considerations, it appears that the form of the mobility equation [Eq. (9)] is able to account for DW dynamics in many practical cases including ultrathin films and microstructural strips. In extreme limits, when H approaches or exceeds the Walker breakdown field, it is necessary to assume that the mobility ξ is strongly dependent on H.

IV. SUMMARY

In summary, this paper presents the first (to our knowledge) direct measurements of BJ velocity distributions in the (thin-film) limit where eddy-current damping is negligible. The measured velocity distributions are confined to a region of $v(H)$ space defined by a maximum DW mobility $\xi'_{\max}$ that is governed by local damping, and compatible with accepted measured parameters for permalloy.

The BJ amplitude distributions $P(\Delta M)$ versus ΔM determined from our microstructured thin-film samples exhibit sweep-rate-dependent power-law behavior with a sharp cutoff region similar to what has been observed in bulk materials where eddy-current damping governs DW velocities. Our microstructured samples are large enough to suppress significant departures from power-law behavior permitting estimates of the scaling exponents. Analysis of $P(\Delta M)$ distributions for four sweep rates based on a uniformly applied power-law fitting criteria covering the same range of ΔM (that neglects the cutoff region) yields an estimate of $\beta \sim 1.5$ at low sweep rates with β decreasing to $\beta \sim 1$ at the highest accessible sweep rate of $dH/dt=6.4\times10^4$ Oe/s. This preliminary result is compatible with the ABBM model, with experimental results on a class of bulk samples, and with measurements of β in permalloy films over a thickness range extending from 3000 to 500 Å. This interpretation based on a dataset having limited dynamic range is also compatible with the sweep-rate inequality relationship that permits sweep-rate-dependent scaling for adiabatic values of $\beta=\frac{3}{2}$.

It was possible to improve the sensitivity and therefore the dynamic range of the $P(\Delta M)$ distribution for the high

temporal resolution measurements at the lowest drive frequency by binning $M(t)$ sampling. The extended range of power-law behavior resulted in a more accurate (and lower) value of β in the adiabatic limit, $\beta=1.28\pm0.02$. This value of β should not allow sweep-rate-dependent scaling, but all reasonable attempts to fit all four measured $P(\Delta M)$ distributions [Figs. 2(b)–2(e)] obtained at high temporal resolution including a reasonable account of cutoff regions failed to allow an interpretation that did not include sweep-rate dependence of β.

Additional experiments conducted on the microstructure and on a 300-Å-thick permalloy film using a more intense laser source (slightly better intrinsic dynamic range) yielded measured values of β in the range of $\beta\sim1.33\pm0.01$ at low sweep rates, and clear evidence of sweep-rate-dependent scaling (Table II). We conclude that, based on all of the results obtained on our permalloy microstructures and thin films to date, the best estimate of β at low frequencies is $\beta=1.33\pm0.01$, which is consistent with the CZDS model with $d=2$, and that sweep-rate-dependent scaling is observed for all data sets independent of whether they favor $d=3$ $\left(\beta=\frac{3}{2}\right)$ or $d=2$ $\left(\beta=\frac{4}{3}\right)$ behavior.

Our results definitively rule out $\beta\sim1$ at low sweep rates corresponding to SOC in $d=2$, which has been reported in other thin-film systems. The primary conclusion regarding the understanding of the BE in thin-film materials, especially the scaling, and critical exponents is that the understanding of these phenomena is very primitive, and that a large amount of systematic work will be required to resolve the apparent inconsistencies and discrepancies. There are reasonably good prospects of advancing the experimental methodology based on MOKE detection of BJ that will permit higher sensitivity measurements, which should allow more definitive interpretation.

Our measured velocity distributions are compatible with general features of the ABBM description of the BE [including the $c\rightarrow0$ jump amplitude exponent for $P(\Delta M)$]. Averaged values of H_p as a function of c (sweep rate) reproduce the frequency dependence of $H_c^*(\omega)$ reported in energy-loss scaling studies of permalloy microstructures. More specifically, the crossover point $c\sim1$ determined from jump-amplitude distributions is associated with a significant change in the shape of the $v(H)$ scatter plots as well as the onset of more rapidly increasing energy-loss scaling. In the $c\gg1$ limit, the distribution functions for $v(H)$ are believed to narrow and cluster around the line that defines the average mobility ξ and $H_c^*(\omega)$.[35] It is clear from the distribution in Fig. 2(e) corresponding to $c\sim0.2$ that this trend has not begun to be manifested, nor is it apparent for $c\sim1$. One point worth mentioning regarding the sweep dependence of the exponents [Eqs. (3)–(5)] is the role played by DW damping. Measurements of bulk samples where eddy-current damping limits mobility detect sweep-rate variation at relatively low sweep rates, whereas our experiments on thin films require rather high sweep rates to detect significant departure of the measured exponent (β in this paper) from the adiabatic limit value. This difference is probably a manifestation of the difference in DW velocities resulting from local (gyromagnetic) versus nonlocal (eddy-current) damping; therefore, the relationship between the sweep-rate dependence of scaling exponents and the dominant DW damping mechanism is a subject that appears to merit additional attention. A final feature of these results is the departure of averaged stochastic velocities [Fig. 5, Eq. (7)] from the linear model Eq. (1). The results presented in this paper clearly demonstrate the limitations of modeling magnetic switching based on a nonstatistical description, even in the sweep-rate range where $c\sim1$.

ACKNOWLEDGMENTS

The authors are pleased to acknowledge valuable discussions with G. Durin and E. Puppin. This work was supported by NSF (NIRT/DMR-0404252), the Texas Coordinating Board (ATP-0099), and by the Robert A. Welch Foundation (F-1015).

[1] G. Durin and S. Zapperi, cond-mat/0404512.
[2] B. Alessandro, C. Beatrice, G. Bertotti, and A. Montorsi, J. Appl. Phys. **68**, 2901 (1990); **68**, 2908 (1990).
[3] P. Cizeau, S. Zapperi, G. Durin, and H. E. Stanley, Phys. Rev. Lett. **79**, 4669 (1997); S. Zapperi, P. Cizeau, G. Durin, and H. E. Stanley, Phys. Rev. B **58**, 6353 (1998).
[4] G. Bertotti, G. Durin, and A. Magni, J. Appl. Phys. **75**, 5490 (1994).
[5] G. Bertotti, *Hysteresis in Magnetism* (Academic, San Diego, 1998).
[6] A. Magni, C. Beatrice, G. Durin, and G. Bertotti, J. Appl. Phys. **86**, 3253 (1999).
[7] C. Nistor, E. Faraggi, and J. L. Erskine, Phys. Rev. B **72**, 014404 (2005).
[8] J. S. Urbach, R. C. Madison, and J. T. Markert, Phys. Rev. Lett. **75**, 276 (1995); **75**, 4694 (1995).
[9] H. J. Williams, W. Shockley, and C. Kittel, Phys. Rev. **80**, 1090 (1950).
[10] R. M. Bozorth, *Ferromagnetism* (VanNostrand Company Inc., New York, 1961).
[11] M. Heidkamp and J. L. Erskine, Rev. Sci. Instrum. **71**, 3141 (2000).
[12] E. Puppin, Phys. Rev. Lett. **84**, 5415 (2000).
[13] L. Callegaro, E. Puppin, and S. Ricci, J. Appl. Phys. **90**, 2416 (2001).
[14] O. Perkovic, K. Dahmen, and J. P. Sethna, Phys. Rev. Lett. **75**, 4528 (1995).
[15] A. Vazquez and O. Sotolongo-Costa, Phys. Rev. Lett. **84**, 1316 (2000).
[16] R. A. White and K. A. Dahmen, Phys. Rev. Lett. **91**, 085702 (2003).
[17] S. L. A. deQueiroz, Phys. Rev. E **69**, 026126 (2004).
[18] P. Bak, C. Tang, and K. Wiesenfeld, Phys. Rev. Lett. **59**, 381 (1987).

[19] N. J. Wiegman, Masters thesis, Technische Universiteit, Eindhoven (results described in Ref. 1).
[20] E. Puppin, S. Ricci, and L. Callegaro, Appl. Phys. Lett. **76**, 2418 (2000).
[21] D.-H. Kim, S.-B. Choe, and S.-C. Shin, Phys. Rev. Lett. **90**, 087203 (2003).
[22] M. Redjdal, J. Giusti, M. Ruane, and F. B. Humphrey, J. Appl. Phys. **91**, 7547 (2002).
[23] Y. Nakatani, N. Hayashi, T. Ono, and H. Miyajima, IEEE Trans. Magn. **37**, 2129 (2001).
[24] T. J. Silva, C. S. Lee, T. M. Crawford, and C. T. Rogers, J. Appl. Phys. **85**, 7849 (1999).
[25] W. K. Hiebert, A. Stankiewicz, and M. R. Freeman, Phys. Rev. Lett. **79**, 1134 (1997).
[26] G. S. D. Beach, C. Nistor, C. Knutson, M. Tsoi, and J. L. Erskine, Nature (London) (to be published).
[27] Y. Nakatani, A. Thiaville, and J. Miltat, Nature (London) **194-196**, 1009 (1994).
[28] S. Konishi, S. Yamada, and T. Kasnda, IEEE Trans. Magn. **MAG-7**, 722 (1971).
[29] P. Vavassori, F. Ronconi, M. Traldi, and E. Puppin, J. Magn. Magn. Mater. **177/178**, 127 (1998).
[30] T. A. Moore, J. Rothman, Y. B. Xu, and J. A. C. Bland, J. Appl. Phys. **89**, 7018 (2001).
[31] W. Y. Lee, B.-Ch. Choi, Y. B. Xu, and J. A. C. Bland, Phys. Rev. B **60**, 10216 (1999).
[32] L. Sauti, R. L. Sommer, A. Magni, G. Durin, F. Colaiori, and S. Zapperi, IEEE Trans. Magn. **39**, 2666 (2003).
[33] I. Lyuksyutov, T. Natterman, and V. Pokrovsky, Phys. Rev. B **59**, 4260 (1999).
[34] M. Kolesik, M. A. Novotny, and P. A. Rikvold, Phys. Rev. B **56**, 11791 (1997).
[35] T. A. Moore, S. M. Gardiner, C. M. Guertler, and J. A. C. Bland, Physica B **343**, 337 (2004).